Naval Research Laboratory

Washington, DC 20375-5320

NRL/MR/7630--14-9510

Observing Short-wave Infrared Atmospheric Fluorescence Near Radioactive Sources: A Feasibility Study

Kenneth D. Marr

NRC Postdoctoral Research Associate
Geospace Science and Technology Branch
Space Science Division

David E. Siskind
Christoph R. Englert
Charles M. Brown

Geospace Science and Technology Branch
Space Science Division

Bernard F. Phlips
Lee Mitchell

High-Energy Space Environment Branch
Space Science Division

March 17, 2014

REPORT DOCUMENTATION PAGE

Form Approved
OMB No. 0704-0188

1. REPORT DATE *(DD-MM-YYYY)*	**2. REPORT TYPE**	**3. DATES COVERED** *(From - To)*
17-03-2014	Memorandum Report	September 2011 – April 2013

4. TITLE AND SUBTITLE

Observing Short-wave Infrared Atmospheric Fluorescence Near Radioactive Sources: A Feasibility Study

5a. CONTRACT NUMBER

5b. GRANT NUMBER
MIPR HDTRA 124655

5c. PROGRAM ELEMENT NUMBER

6. AUTHOR(S)

Kenneth D. Marr,[1] David E. Siskind, Christoph R. Englert, Charles M. Brown, Bernard F. Phlips, and Lee Mitchell

5d. PROJECT NUMBER

5e. TASK NUMBER

5f. WORK UNIT NUMBER
76-4184-32-5

7. PERFORMING ORGANIZATION NAME(S) AND ADDRESS(ES)

Naval Research Laboratory, Code 7630
Space Science Division
4555 Overlook Avenue, SW
Washington, DC 20375-5320

8. PERFORMING ORGANIZATION REPORT NUMBER

NRL/MR/7630--14-9510

9. SPONSORING / MONITORING AGENCY NAME(S) AND ADDRESS(ES)

Defense Threat Reduction Agency
Ft. Belvoir, VA 22060

10. SPONSOR / MONITOR'S ACRONYM(S)

DTRA

11. SPONSOR / MONITOR'S REPORT NUMBER(S)

12. DISTRIBUTION / AVAILABILITY STATEMENT

Approved for public release; distribution is unlimited.

13. SUPPLEMENTARY NOTES

[1]NRC Postdoctoral Research Associate

14. ABSTRACT

We attempted to image atmospheric fluorescence in the short-wave infrared (SWIR) from several radioactive sources. Our detection system was an InGaAs camera, fitted with a 25 mm lens to image the scene. No definitive fluorescence was detected. We also used our system to observe the SWIR emission from a proton beam source and established certain criteria for use as fluorescence diagnostics. For example, we clearly observed an enhancement at 1050 nm relative to 1600 nm, consistent with known emission features of molecular nitrogen and with previously published results. However, even for a high activity cobalt-60 source, our recorded signal was not consistent with these diagnostics. Rather, we hypothesize that the small signal which was recorded may have been due to direct incidence of gamma rays on our detector. Compared with the ultraviolet (UV), the infrared emission is expected to be only 20% as bright. We suggest that to increase the signal to noise in the SWIR may require either a telescope to collect a greater fraction of the emission or to image a more localized source than the gamma emission. Further research should include coincident UV and SWIR observations.

15. SUBJECT TERMS

Short wave infrared radiation fluorescence
Radioactivity

16. SECURITY CLASSIFICATION OF:			**17. LIMITATION OF ABSTRACT**	**18. NUMBER OF PAGES**	**19a. NAME OF RESPONSIBLE PERSON**
					David E. Siskind
a. REPORT	**b. ABSTRACT**	**c. THIS PAGE**	Unclassified Unlimited	18	**19b. TELEPHONE NUMBER** *(include area code)*
Unclassified Unlimited	Unclassified Unlimited	Unclassified Unlimited			(202) 767-0928

Contents

1 Introduction

Stand-off detection of radioactive sources is of interest for both military and civilian applications. One potential method of detection is the observation of atmospheric fluorescence that occurs as the radiation from active sources impacts the surrounding air. Historically, scientific interest in atmospheric fluorescence from energetic particle impact has been motivated by a desire to measure cosmic ray effects. For example, the pioneering study of cosmic ray detection by fluorescence was by Bunner in 1967 wherein he detected specific N_2 emission features in the near UV [1]. Motivated by some discrepancies as well as the need to measure a broader range of wavelengths, the ultra-high energy cosmic ray (UHECR) community has continued to pursue studies of the fluorescence yield from high energy particle impact on N_2 and air [2, 3]. With regard to fluorescence from terrestrial radiation sources, the University of Southern Mississippi has conducted studies using stand-off detectors sensitive to the UV spectrum [4]. Ultraviolet fluorescence efficiencies (photons produced per decay) have been calculated for both α- and β-radiation [4, 5].

Recently, interest has shifted towards the potential of using the short-wave infrared (SWIR) wavelength region to observe atmospheric fluorescence. One of the main reasons for this interest is that the atmosphere is more transparent to infrared (IR) photons than to ultraviolet (UV) photons. This potentially allows for detection at greater distances than could be achieved using UV detectors. However, one drawback of this effect is that during day-time (outdoor) detection the background scene would contain significantly more IR photons than UV photons. In this sense, UV detection is "solar blind." Furthermore, Nagano *et al* [5] used atmospheric fluorescence from electrons produced though strontium-90 β-decay to observe that the photon yield in the UV spectrum is nearly five times that in the IR spectrum. It was also shown that fluorescence yield in air is less than in pure N_2; an effect thought to be the result of quenching of the excited N_2 by molecular oxygen. Similarly, Conti *et al* [6] used an InGaAs photodiode to observe the emission spectrum from a beam of electrons produced by an electron accelerator. They found that the peak emission of SWIR fluorescence was concentrated in the spectral range from 1050 nm – 1350 nm.

We were tasked with studying the feasibility of using SWIR detection to observe atmospheric fluorescence from terrestrial radiation sources. We approached the question with both an examination of the literature and with laboratory experiments using a near infrared (NIR) camera. We conducted three experiments to try to observe infrared fluorescence from 1) low activity radioactive sources ($\ll$ 1 Ci) in the laboratory, 2) a proton accelerator at the University of Massachusetts at Lowell (UMass - Lowell), and 3) a high activity cobalt-60 source ($\sim$60 Ci). In this report, Section 2 describes the characterization of the InGaAs camera, including background subtraction and quantum efficiency. Section 3 provides the results from the low activity sources. Section 4 describes the proton fluorescence observations with an emphasis on validating

Manuscript approved January 23, 2014.

key diagnostics, i.e. identifying particular signatures of SWIR atmospheric fluorescence. In Section 5 we apply these diagnostics towards imaging part of the emission from the cobalt-60 source and conclude that even though there was an increase in signal, we did not observe fluorescence. In Section 6 we discuss the literature and the overall feasibility of the ultimate goal of detecting radiation sources using SWIR fluorescence. Section 7 provides an executive summary of the work performed.

2 Camera Characteristics

Data for the experiments was collected with a Xeva 377 InGaAs camera from XenICs Inc. The camera was controlled with the Xeneth software package (v2.4) also provided by XenICs Inc. A Navitar infrared lens (#SWIR-25) with a focal length of 25 mm was fitted to the front of the camera to image the scenes.

Before imaging any fluorescence from radioactive sources we characterized the camera using an infrared light source. The chosen light source was a commercially available, clear, red-glass light bulb running at a very low voltage to produce IR photons. At 2 – 5 V no visible light could be seen, but sufficient IR photons were detected for calibration. Nearly flat images were generated by inserting the light source into a $10''$ integrating sphere (LabSphere), which through multiple internal reflections produces a uniform field at the output port.

The camera control software has several parameters which affect the relative scale of the returned camera data, i.e. the Analog to Digital Units (ADU), or counts, returned when a specific number of photons strike the collection area. The first parameter is the offset voltage, V_{in}. The second parameter is the reference voltage, V_{ref}. The combined adjustment of these two values allows for the optimization of the scale for a specific range of intensities. The third value is the detector voltage, V_{det}, however this value was not changed throughout this study. The camera parameters were typically set so that the full well-depth (dynamic range) of the InGaAs detector was accessible. The camera is operated in one of two modes, low-gain or high-gain, which determines the CCD signal multiplication factor.

For this camera, the variation of signal offset between neighboring pixels is significant. Typically, this offset non-uniformity is manifested as vertical lines on the image. This variation is replicated in any dark frame (one with the same integration time and no light sources) and can be removed during analysis. Figure 1 shows an example of this process. Figure 1a shows the raw image of the low-voltage infrared light source (bulb) which has been almost completely covered in aluminum foil. The white spot is where the infrared light exits the cover. Figure 1b shows the same scene after we have subtracted a corresponding dark image. The vertical streaking seen in the raw data has been eliminated via this process. Background subtraction has the added benefit of improving the contrast in the false-color image.

Through analysis of the images taken with the integrating sphere, we found that in low-gain mode the detector response was non-linear as a function of

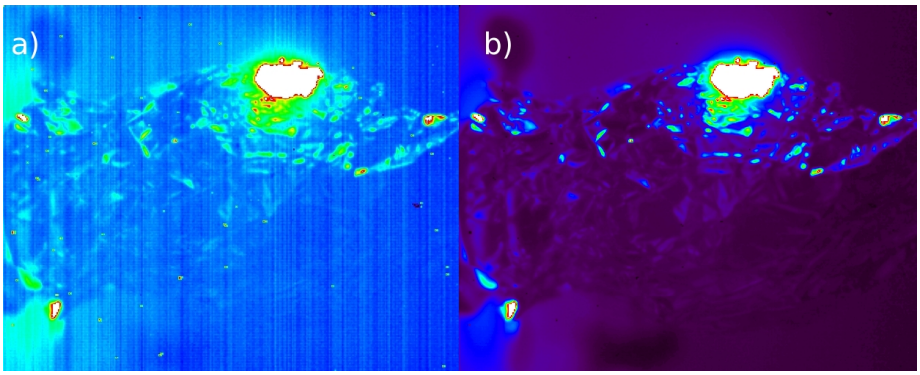

Figure 1: a) Image of the infrared light source (low voltage light bulb wrapped in aluminum foil) before background subtraction. Pixel to pixel variation (flat-field) is seen as vertical streaking. b) Same image after the background is subtracted.

integration time, i.e. signal. Without a deeper understanding of the processes internal to the camera, such as the detector read out, we were unable to ascertain the cause of this non-linearity. However, it is possible, for any given set of camera parameters, to account for this non-linearity during analysis when multiple signal levels need to be compared. In contrast, the camera response in high-gain mode was nearly linear with signal.

We estimated the camera's sensitivity to photons by using the signal to noise ratio from the measurement of a constant light source. Assuming counting statistics (shot noise) dominates over the read out noise (noise generated by the electronics as each frame of data is pulled from the camera), the ratio of the signal, S, to the standard deviation of the noise, σ, in ADU, should be equal to the square root of the number of photons counted,

$$S_{\mathrm{ADU}}/\sigma_{\mathrm{ADU}} = \sqrt{N_{\mathrm{photons}}}. \tag{1}$$

To determine the standard deviation of the noise inherent in a single image we must isolate the noise from the pixel to pixel offset variation. However, any measurement of the offset variation will also have a similar but independent amount noise, σ_{off}. When subtracted, the standard deviations of these noises will add in quadrature. Thus, after subtracting the offset variation from a given frame of data we get a total standard deviation of

$$\sigma_{\mathrm{total}} = \sqrt{\sigma^2_{\mathrm{ADU}} + \sigma^2_{\mathrm{off}}} = \sqrt{2}\sigma_{\mathrm{ADU}}. \tag{2}$$

Solving Equation (1) for the number of photons counted and dividing by the number of counts generated, S_{ADU}, we derive a conversion factor, f, between photons and counts,

$$f \equiv N_{\mathrm{photons}}/S_{\mathrm{ADU}} = S_{\mathrm{ADU}}/\sigma^2_{\mathrm{ADU}}. \tag{3}$$

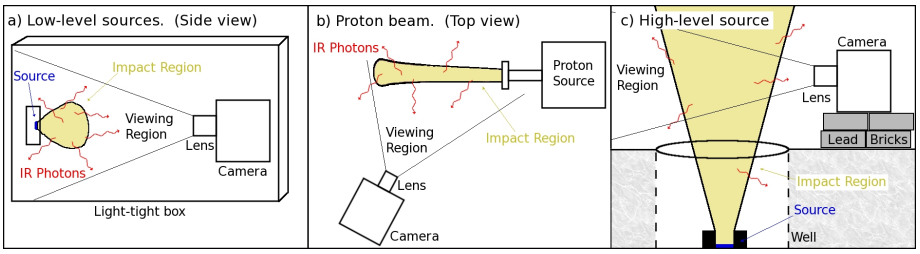

Figure 2: (Not to scale.) Viewing schematics for a) the low activity sources, b) the proton beam at UMass - Lowell, and c) the high activity cobalt-60 source.

In low-gain mode we find that several hundred photons are required to generate one ADU. We determine the conversion factor to be between $300 < f < 500$ photons/ADU, increasing with total detected signal. This behavior is likely due to the non-linearity of the system in low-gain operation that was discussed above or due to variations of the light source.

High-gain mode has an experimentally determined value of approximately $f = 55$ photons/ADU, which is a marked improvement over the low-gain value when counting a low number of photons. With higher gain the integration time becomes limited to several seconds in order to not saturate the camera with dark current (counts generated over time by the detector when no light sources are present). Thus, multiple frames are required for the same integration time as a single, long, low-gain image. Nonetheless, even with the addition of read-noise from multiple read outs, the increase in signal to noise makes high-gain the operational mode most likely to detect infrared photons from a faintly radiating source.

3 Low Activity Source Results

This study began with an examination of low activity ($\ll 1$ Ci) sources. To reduce background signal collected during observation of the fluorescence generated by these radioactive sources, the camera was enclosed in a light-tight box. Though able to prevent visible light from entering the camera, some background infrared radiation and usual dark current would still accumulate on the camera detector array during imaging. The radioactive sources examined, their radiation type, and their activities are listed in Table 1.

Figure 2a shows a schematic of the laboratory setup for the radiation sources with low-levels of activity. For the results presented here, the sources were oriented head-on to the line of sight from the camera so that the radiation would impact the air between the source and camera. The α-particles emitted by the thorium source are expected to deposit their energy within the first few centimeters of atmosphere while the γ-rays from the other sources will deposit their energy over significantly larger distances comparatively. Figure

Source	Radiation Type	Activity
Thorium-228	α-particles	0.19 μCi
Cesium-137	γ-rays	0.92 mCi
Cesium-137	γ-rays	7.3 mCi
Americium-241 (sealed)	γ-rays	11 mCi

Table 1: Low-power radioactive sources examined in the light-tight box.

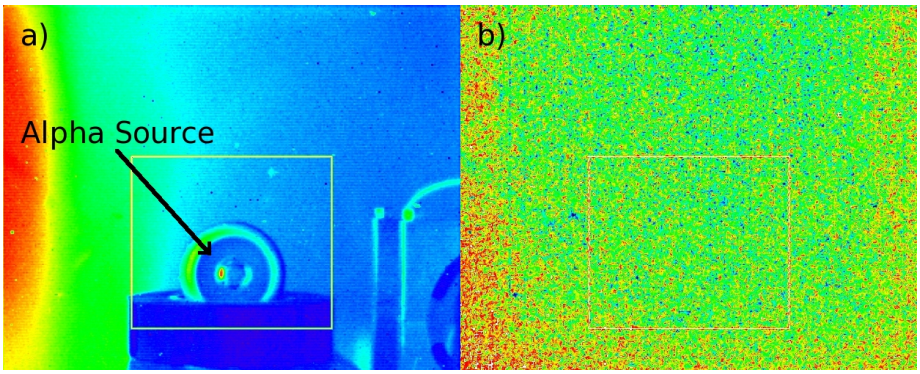

Figure 3: a) The illuminated α-source pointing directly at the camera. b) The aggregate image of the source in the darkened box with background subtracted. Data was collected for over 17 hours. The slight increase in counts around the bottom and side edges is determined to be a remnant from the background removal process.

2a is not to scale and the camera was located ~0.5 m away from the source. Tests were also performed with the source laying flat, emitting decay particles roughly perpendicular to the camera's line of sight, but there was no difference in results.

As a first experiment, the α-particle source was imaged in low-gain mode for over 17 hours in 30 s increments. A corresponding background image was subtracted from each 30 s image and the results were aggregated into a single, averaged image. No fluorescence signature was detected. Similar experiments were run in high-gain mode with 3 s exposures. Figure 3a shows a false color, head-on image of the α-source while the scene is externally illuminated. The source is the small circle inside the cylindrical container (outer ring). A yellow square has been drawn around the source for ease of reference. Figure 3b shows the aggregate, background subtracted image of the source while the lights are off. There appears to be some increased signal on the left, right, and bottom sides of the image in Figure 3b. However, because this effect was localized in time to early in the experiement and due to the fact that it does not make a symmetric pattern around the α-particle source, we find it to be unrelated to

the source, but rather an effect from background removal. Furthermore, the background images for this test were taken well after the 17 hours of source imaging and changes in room temperature may therefore have had an effect.

The cesium and americium sources were also imaged (for < 1 hr each), but also did not show any obvious fluorescence signals. These γ-ray sources were also viewed head-on. The 662 keV γ-rays from the cesium sources have a half energy distance of 100 m. Therefore, in the 50 cm between the source and the camera we would expect only 0.3% of the γ-rays to have been absorbed by the atmosphere. Furthermore, due to the geometry of the experiment, the impact region is a cone originating at the source and completely filling the camera optics. Thus, detection of the source would be seen as an overall increase in signal across the entire detector array rather than a subset of pixels as might be expected for the α-particle source.

4 Proton Beam Results at UMass – Lowell

Here we describe the observations of the proton beam at the University of Massachusetts - Lowell and quantify it's emission efficiency. Since the atmospheric fluorescence from the protons was relatively bright and easily detectable, we also use this opportunity to define specific diagnostics, or benchmarks, to characterize SWIR fluorescence. These benchmarks are applied in Section 5 where we discuss results from the observation of a cobalt-60 source.

The three diagnostics developed were

1. the extent of the impact region based on the energy of the protons,
2. the ratio of emission intensity between 1050 nm and 1600 nm, and
3. the relative emission intensity in air vs. pure nitrogen.

Figure 2b shows a cartoon schematic of the camera and proton beam (not to scale). The line of sight from the camera was $\sim 90^\circ$ to the beam path and far enough away from the port ($\sim$1 m) to image the entire beam length.

Figure 4 shows four false-color images from a series of experiments at different energies (which affects the length of the beam) and currents (which affects the intensity of beam). The beam originates at the port which is represented by an oval-shaped signal enhancement on the right side of each panel in Figure 4. The energies are approximate and the current varied significantly due to machine limitations, meaning that any values reported are rough averages over several seconds. Beam focusing and other parameters besides current also affect the relative intensity between experiments with different energies. Despite these uncertainties, Figure 4 clearly shows that higher energies travel further. The 4 MeV proton beam traveled about 1.6 times further than the 3 MeV beam with the 3.3 and 3.5 MeV beam lengths in between. This is in excellent agreement with Sternheimer's calculations of expected proton penetration in air [7].

We also tested the effective "color ratio" of SWIR fluorescence by observing the beam through two filters. Previous work suggested a concentration of atomic

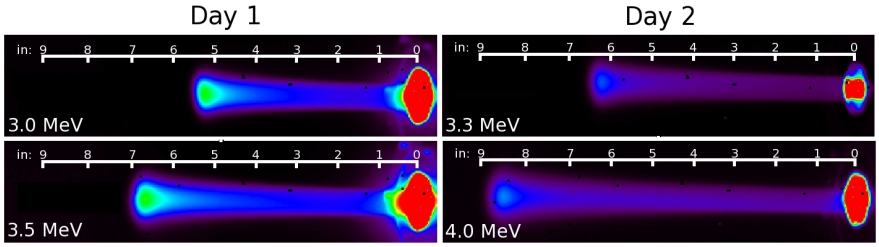

Figure 4: Four representative false-color images of the UMass - Lowell proton beam experiments. The images on the left were taken on the first day of operation are have energies of 3.0 MeV and 3.5 MeV, respectively. Day 2 images on the right have 3.3 MeV and 4.0 MeV, respectively. The images from Day 2 appear "dimmer" due to color-scaling and different beam currents.

and molecular emission lines yielding peak emissions near 1045 nm [6]. Our results are consistent with this. Using commercial filters with center wavelengths of 1050 nm and 1600 nm and full-widths at half max (FWHM) of 10 nm and 12 nm, respectively, we isolated these portions of the spectrum. Figure 5 shows the results of this experiment. Unfiltered, the camera is sensitive from about 900 nm – 1700 nm and has a peak-above-baseline value (baseline being determined by the signal between 0 and 50 pixels) of just over 900 counts for a 1 s integration. Although the spectral bandpass of these filters represent less than 2% of the unfiltered bandwidth, it can be seen that when using the 1050 nm filter, the peak-above-baseline value has fallen to ∼100 counts, or ∼11% of the unfiltered peak signal. Thus, we verify that a significant amount of the fluorescence within the spectral sensitivity of the camera is located in the wavelength band near 1050 nm. There are no significant atmospheric fluorescence lines around 1600 nm and correspondingly, minimal signal is visible above the background when this filter was in use.

Finally, it has been observed that the presence of oxygen will reduce the total signal in the UV and IR wavelength ranges when observing fluorescence from electron impact [6, 5]. This is assumed to be due to the presence of oxygen modifying or eliminating certain relaxation paths for excited nitrogen. To verify this effect with the proton source, we enclosed the beam and camera in a nearly pure nitrogen environment. Figure 6 shows a comparison of the fluorescence for two energies and current combinations. Comparing the signal strength for the case in the pure nitrogen environment with that in a standard atmosphere, we see a clear enhancement of signal along the length of the emission. The average value of the increase is a factor of 2 – 3. While significant, this enhancement is less than the factor of 5 – 8 seen in previous UV experiments [4, 5]. It is possible that some residual oxygen might have persisted in the enclosed area, which was purged with a constant nitrogen flow. On the other hand, since no other quantitative observations of this effect have previously been made in the

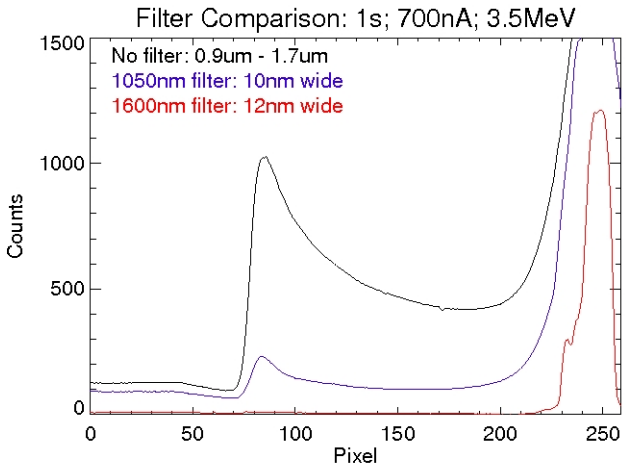

Figure 5: Total counts per column (pixel) of the UMass - Lowell proton beam with no filter (black), 1050 nm filter (blue), and 1600 nm filter (red). The beam port can be seen as a bright area above 200 pixels.

SWIR region, this discrepancy may simply reflect differing quenching rates of the SWIR emission bands.

Using the estimated current, it is possible to derive a rough proton fluorescence efficiency, $\epsilon_{\rm p} = N_{\rm ph}/N_{\rm p}$, where $N_{\rm ph}$ is the number of photons emitted and $N_{\rm p}$ the number of protons. Assuming the camera is 1 m away from the beam, it collects about 0.02% of the photons being emitted. Using this geometrical factor and $f = 55$ photons/count as determined above, we convert total counts collected to $N_{\rm ph}$. We calculate $N_{\rm p}$ emitted by the source by using the estimated current. Table 2 shows the results of these calculations. Also shown is the number of photons produced per proton per energy. It should be noted that whenever the energy of the beam was changed, it was also necessary to adjust the gap size of the beam limiter. This could explain the inconsistencies between the results from experiments 1 – 3 in Table 2, which were taken on the first day, and those from experiments 4 – 7, which were taken on the second day. Thus, any comparison between the results has a significant associated uncertainty. However, we can give an order of magnitude estimate of the overall efficiency ($10^{-2} < \epsilon < 10^{-1}$) as well as highlight a few trends. Specifically, the efficiency generally increases with energy as well as increases with nitrogen concentration. Again, we see the increase between a pure nitrogen environment and regular atmosphere is a factor of 2 – 3 for the infrared.

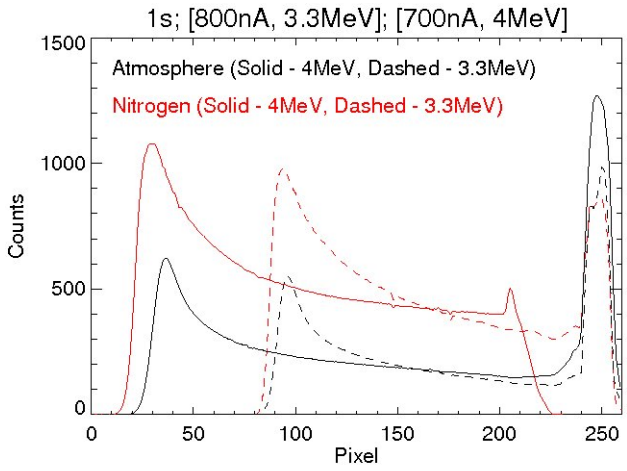

Figure 6: Total counts per column (pixel) of the UMass - Lowell proton beam in both atmosphere (black) and nitrogen (red). Solid lines represent 4.0 MeV and dashed lines represent 3.3 MeV. The beam port can be seen as a bright area above 200 pixels except for 4.0 MeV in nitrogen, which was cut off from view by the enclosure.

5 High Activity Cobalt-60 Source Results

With our fluorescence diagnostics validated during the Lowell observations, we attempted to measure fluorescence from a high activity cobalt-60 source. Due to the high activity of the cobalt source, it was required that the source be kept in a lead-lined well for the protection of nearby personnel. Figure 2c shows a cartoon of the source in this well. The γ-rays travel up out of the well, perpendicular to the line of sight from the camera. When not observed the source is lowered to a depth of 500 cm and the well covered with lead bricks. When observed, the source was elevated to a depth of roughly 60 cm. With the camera situated near the edge of the well, the impact region fills the viewing area. Similar to the low activity γ-sources, we are only viewing a small fraction (25 cm) of the half-energy length traveled by the 1173 keV γ-rays (200 m). This means that $< 0.1\%$ of the total energy is deposited in the viewing region.

Figure 7 shows the results from the experiments viewing the cobalt-60 source. When the source was elevated and uncovered there was an increase in average signal per pixel no matter where the camera was located. However, to classify this signal increase as atmospheric fluorescence, it must satisfy the diagnostics developed while observing the fluorescence from the UMass - Lowell proton beam as described in the previous section. Specifically, we expect a significant portion of the signal to be in a 20 nm band around 1050 nm and essentially no signal to be in the 20 nm band around 1600 nm. For the cobalt experiment, when the

	Current (nA)	**Env.**	**Energy** (MeV)	**IR Photons proton**	**IR Photons proton · MeV**
1	500	Air	4.0	0.055	0.014
2	700	Air	3.0	0.039	0.013
3	700	Air	3.5	0.060	0.017
4	800	Air	3.3	0.021	0.006
5	800	N_2	3.3	0.052	0.016
6	700	Air	4.0	0.039	0.010
7	700	N_2	4.0	0.095	0.024

Table 2: Photons per proton and photons per proton per energy for the UMass - Lowell experiments. Experiments 1 – 3 were performed on the first day while 4 – 7 are from the second day.

filters were in use, there was no decrease in signal nor did the signal depend on wavelength. Neither was there a strong signal dependence on distance between 25 cm, 50 cm, and 3 m (not shown). It is our estimation that scattered γ-rays are penetrating through the lens and filters, to interact with the detector array. This theory is supported by the increased number of saturated pixels (hot spots) when the source is elevated. At the levels measured (a difference of 3 – 10 counts on a signal of 2800 counts) using an accurate background during analysis is extremely important. The lower signal seen during the first test (no filter at 25 cm) as compared to later tests is likely due to the changing background conditions in the room. Because simultaneous background measurements were impossible, the background used in the analysis of each signal image was interpolated from background measurements taken before and after the data was collected.

6 Discussion

Here we discuss prior experiments performed with the goal of detecting radiation sources as well as determine the minimum activity required for stand-off detection of a theoretical strontium-90 β-source during a 2 s integration.

Recently, there have been a few experiments using radioactive sources rather than cosmic rays to study atmospheric fluorescence [4]. In one experiment, an americium-241 source with a strength of 100 μCi was viewed from a distance of 36.8 cm with a photomultiplier tube of area 491 mm^2 in both air and N_2. This measurement indicated a UV fluorescence efficiency of 3.6×10^{-7} photons/decay in air and 2.8×10^{-6} photons/decay in N_2. Accounting for the 5:1 factor between UV and IR fluorescence and using the definition of activity, 1 Ci $= 3.7 \times 10^{10}$ decays/s, we estimate the thorium source studied at the Naval Research Laboratory (NRL, see Table 1), which is over 500 times weaker than the americium source, should produce roughly 5×10^{-4} IR photons/s radiating into 4π. If we generously assume we collect all of these photons (and ignore

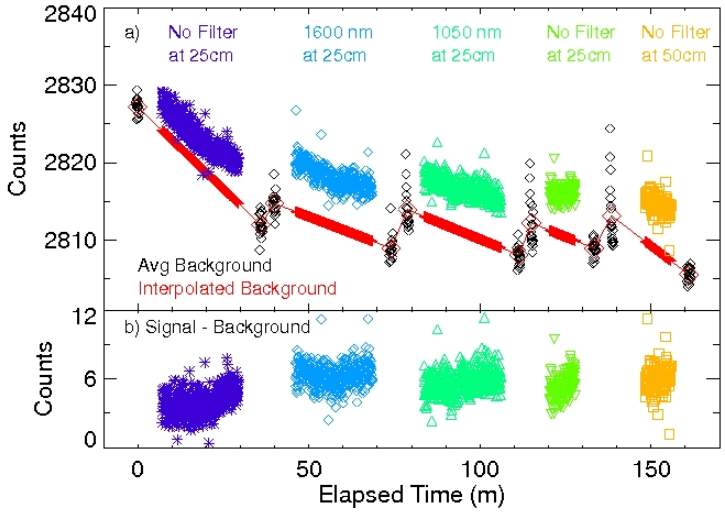

Figure 7: Results from observations of the high activity cobalt-60 source. a) Raw data showing average over the whole CCD for the five experiments and associated backgrounds (before and after each experiment). Averages of the interpolated backgrounds are also shown (red). b) The remaining signal after interpolated backgrounds have been subtracted. Of the five tests performed, three were done with no filter: two tests at 25 cm and one test at 50 cm. The other two tests were with the 1050 nm filter and the 1600 nm filter, both at 25 cm away.

saturation by dark noise) we would still need 100,000 s to see enough photons to generate a single count on the current camera. In reality, the camera used in this study (and any camera that does not observe a solid angle of 4π) would collect only a small fraction of these photons (0.1% assuming 36.8 cm from the source with a 5 cm diameter lens). Note that while we observed an americium source at NRL which is significantly more active than the americium that was used as an α-source by [4], the NRL source is shielded to α-particle emission (sealed) and therefore only functions as a source of its secondary decay product, γ-rays.

To estimate the strength of a strontium-90 β-source that would be required for detection by the camera used in this study, let us assume that the source is located in the center of our viewing region. This source produces 0.85 MeV electrons, which are expected to deposit the bulk of their energy within 3 m of the source [8]. In fact, as the electrons lose energy they become more likely to interact with the atmosphere, resulting in a comparatively large and rapid loss of energy furthest from the source. This localized energy deposition is referred to as the Bragg peak. However, the electron density is greatest nearest to the

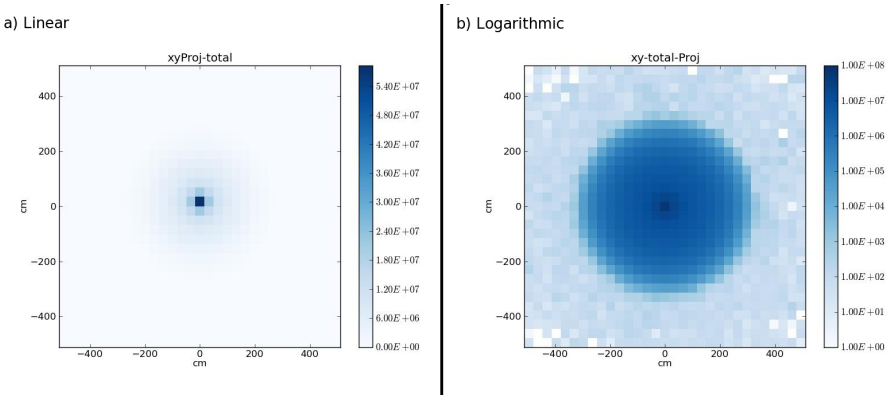

Figure 8: 2D energy density plots from a simulation of a strontium-90 source emitting 1×10^6 electons into air. Results are shown in both a) linear scale and b) logarithmic scale.

source. Combining these two factors we find that the total energy density is also highest near the source. Figure 8 shows the energy density results (both linear and logarithmic) from a simulation of a point source radially emitting 1×10^6 electrons into air. The central box in Figure 8a has a size of 33 cm $\times$ 33 cm and has the highest energy density. Thus, for optimal signal detection, we assume our viewing region to be a circle with a diameter of 33 cm. Let us also assume that the detector is 320 pixels $\times$ 320 pixels, which is larger in one dimension than the actual camera detector. Given the camera optics' magnification, we estimate the camera must be placed just over 1 m away to attain the desired viewing region size.

For our camera, the combination of dark and read out noises for a 2 s exposure which has had an associated dark frame subtracted, has a standard deviation of roughly $\sigma_a = 10$ counts for each pixel, a. If we sum all the pixels into a single value the noise would increase by a factor of 320 while the signal, S, increases by a factor of 1×10^5. Thus, for N illuminated pixels with the identical signal and statistically independent noise of consistent magnitude, we find

$$\sigma_{\text{total}} = \sqrt{\Sigma_a^N \sigma_a^2} = \sqrt{N}\sigma_a, \tag{4}$$

$$S_{\text{total}} = \Sigma_a^N S_a = N S_a. \tag{5}$$

For the scenario described above and considering only the pixels illuminated by the circular viewing region (less than the full array by a factor of $\pi^{1/2}$), $\sigma_{\text{total}} = \sqrt{(1 \times 10^5)/\pi^{1/2}} * 10$ counts $= 1800$ counts. Dividing by the integration time, t, we find, for a desired signal to noise ratio of unity ($S/\sigma \equiv 1$), the necessary collection rate, R, over the whole illuminated area is

$$R_{\text{counts}} = \frac{S_{\text{total}}}{t} = \frac{\sigma_{\text{total}}}{t} = \frac{1800 \text{ counts}}{2 \text{ s}} = 900 \ \frac{\text{counts}}{\text{s}}. \tag{6}$$

Using the high-gain photon counting efficiency ($f = 55$ IR photons/count) calculated in Section 2 we find,

$$R_{\mathrm{IR}} = R_{\mathrm{counts}} * f = \left(900 \frac{\mathrm{counts}}{\mathrm{s}}\right)\left(55 \frac{\mathrm{photons}}{\mathrm{count}}\right) = 5 \times 10^4 \frac{\mathrm{IR\ photons}}{\mathrm{s}}. \quad (7)$$

Note that this ignores the fact that each pixel cannot produce a fractional count. Assuming the camera is 1 m away from the impact region and has an opening diameter of 5 cm, we calculate the fraction of photons reaching the optics based on the given geometry, g, as,

$$g = \frac{A_{\mathrm{camera}}}{A_{\mathrm{surface}}} = \frac{\pi(2.5\ \mathrm{cm})^2}{4\pi(1\ \mathrm{m})^2} = 1.6 \times 10^{-4}. \quad (8)$$

Thus, the total amount of IR photons which must be generated in the viewing region would be

$$R_{\mathrm{IR,total}} = \frac{R_{\mathrm{IR,collected}}}{g} = \frac{5 \times 10^4\ \mathrm{photons/s}}{1.6 \times 10^{-4}} = 3 \times 10^8 \frac{\mathrm{IR\ photons}}{\mathrm{s}}. \quad (9)$$

Using the conversion factor found in the work by Conti *et al* [6], we find

$$R_{\mathrm{UV,total}} = R_{\mathrm{IR,total}} * \frac{5\ \mathrm{UV\ photons}}{\mathrm{IR\ photon}} = 1.5 \times 10^9 \frac{\mathrm{UV\ photons}}{\mathrm{s}}. \quad (10)$$

Although the fluorescence efficiency derived from the work by Nagano *et al*, $\epsilon = 3.6$ UV photons/(electron m) [5], is valid only over small distances ($\sim$5 cm), we may convert this to an efficiency per energy by using a simulation to determine the energy lost over that distance. This energy deposition is found to be $\tau = 180$ keV/m. Combining these two, we derive a fluorescence efficiency per energy lost, $\epsilon_{\Delta \mathrm{E}}$, that is valid over the full length of travel,

$$\epsilon_{\Delta \mathrm{E}} = \frac{\epsilon}{\tau} = \frac{3.6\ \frac{\mathrm{UV\ photons}}{\mathrm{electron\ m}}}{180\ \frac{\mathrm{keV}}{\mathrm{m}}} = 0.02\ \frac{\mathrm{UV\ photons}}{\mathrm{electron\ keV}}. \quad (11)$$

Thus, viewing only the emission from energy deposition in the first 33 cm ($\Delta E = 58$ keV), we derive an electron emisson rate, R_e, of

$$\begin{aligned} R_e &= \frac{R_{\mathrm{UV,total}}}{\epsilon_{\Delta E} * \Delta E} = 1.5 \times 10^9 \frac{\mathrm{UV\ photons}}{\mathrm{s}} \Big/ \left(0.02\ \frac{\mathrm{UV\ photons}}{\mathrm{electron\ keV}} * 58\ \mathrm{keV}\right) \\ &= 1.3 \times 10^9 \frac{\mathrm{electrons}}{\mathrm{s}}. \end{aligned} \quad (12)$$

Assuming each decay from the strontium source generates one electron, this electron emission rate corresponds to an activity, A, of

$$R_e \rightarrow A = 1.3 \times 10^9 \frac{\mathrm{electrons}}{\mathrm{s}} * \frac{\mathrm{Ci}}{3.7 \times 10^{10}\ \mathrm{decays/s}} = 35\ \mathrm{mCi}. \quad (13)$$

Thus, we estimate a minimum activity of 35 mCi is required for bulk detection of an unshielded strontium-90 β-source.

The above calculation makes several assumptions. First we assume only a 2 s integration time. Depending on the strength of the signal, it is possible to perform longer integrations without saturation, which would increase both the signal collected and the noise. The increase in signal would be greater than the increase in noise, resulting in a net benefit. Second, we assume we are summing over several thousand pixels. If resolution of the width of one pixel is desired, a 8 Ci source would be required to generate enough photons for analysis. Conversely, a larger viewing area would reduce the required activity by a factor of $\sqrt{\Delta N}$ where ΔN is the increase in number of pixels illuminated. Finally, the viewing area was assumed to include only a small portion of the impact region of the 0.85 MeV electrons. To view the full energy deposition region (6 m diameter) with our current camera, we would have to place it nearly 20 m away. Although, we would gain signal from the rest of the impact region seen in Figure 8b, we would lose a factor of $(20\text{ m})^2 = 400$ due to the geometry of the optics. Thus, we would need a 870 mCi source to obtain a signal to noise ratio of unity at this distance. The limiting factor in this situation is the small entrance optics. If we were to install a wide angle (fish-eye) lens that allowed the whole impact region to be imaged from a distance of 1 m, then we would only need a 2.5 mCi source to provide the desired signal.

7 Summary

We have attempted to image atmospheric fluorescence in the SWIR from both low and high activity radioactive sources with an InGaAs camera. No definitive fluorescence was detected. We used the SWIR emission from the proton beam accelerator to establish certain criteria for use as diagnostics during detection of fluorescence. Despite a small increase in signal observed when the camera was exposed to radiation from the high activity cobalt-60 source, that increase did not meet these criteria. Specifically, there was no enhancement at 1050 nm relative to 1600 nm. Rather, we suggest that the small signal increase was due to the interaction of direct incidence γ-rays with our detector. It remains a puzzle why no signal was seen from the high activity γ-ray source. In principle, we would be more likely to detect fluorescence if the cobalt-60 source at NRL could be imaged from tens of meters away with no other nearby infrared sources. The calculation of the requisite β-source strength detectable by our system illustrates the importance of the optical system in atmospheric detection. Depending on the distance away from the source (1 m – 20 m) and the lens' field of view, we estimate the minimum detectable activity level to be anywhere between 2.5 and 870 mCi. One recommendation for future studies would be to place both UV and IR detection systems together to simultaneously image the same source.

Acknowledgements

The authors would like to thank Neil Johnson, Richard Woolf, Lori Jackson, the rest of the High Energy Space Environment group, Kim Lister, and the staff at the Radiation Laboratory at the University of Massachusetts - Lowell for their help, advice, and support of this project. This project was funded by the Defense Threat Reduction Agency (DTRA).

References

[1] Bunner, A. N., (1967), Cosmic ray detection by atmospheric fluorescence, PhD. Thesis, Cornell University

[2] Colin, P. et al., (2007) Measurement of air and nitrogen fluorescence light yields induced by electron beam for UHECR experiments, Astropart Phys., 27, 317-325.

[3] Lefeuvere, G., et al. (2007) Absolute measurement of the nitrogen fluorescence yield in air between 300 and 430 nm, Nucl Instr. Meth in Phys., doi:10.1016/j.nima.2007.04.106

[4] Hoff, O. (2012) Determination of Alpha Radiation-Induced Fluorescence Efficiency, B.S. Thesis, University of Southern Mississippi.

[5] Nagano, M., (2003) Photon yields from nitrogen gas and dry air excited by electrons, Astropart. Phys. 20, 293-309.

[6] Conti, E., et al., (2010) Measurement of the near-infrared fluorescence of the air for the detection of ultra-high-energy cosmic rays, Astropart. Phys.

[7] Sternheimer, R. M., (1959) Range-Energy Relations for Protons in Be, C, Al, Cu, Pb, and Air, Phys. Rev., 115 (1) 137-142.

[8] Chamberlain, J. W., (1961) Physics of the Aurora and Airglow, Academic Press Inc., New York, NY.